Phosphorylation on PstP regulates cell wall metabolism and antibiotic tolerance in *Mycobacterium smegmatis*

Farah Shamma[1], Kadamba Papavinasasundaram[2], Samantha Y. Quintanilla[1], Aditya Bandekar[2], Christopher Sassetti[2], and Cara C. Boutte[1]*

[1]Department of Biology, University of Texas Arlington, Arlington, Texas

[2]Department of Microbiology and Physiological Systems, University of Massachusetts Medical School, Worcester, Massachusetts

*corresponding author: cara.boutte@uta.edu

Running title: Phosphorylation of PstP affects the cell wall

Key words:

PstP, Serine/Threonine Phosphatase, peptidoglycan metabolism, mycolic acid metabolism, antibiotic tolerance, Mycobacteria, dephosphorylation, starvation, cell wall metabolism, CwlM

Abstract

Mycobacterium tuberculosis and its relatives, like many bacteria, have dynamic cell walls that respond to environmental stresses. Modulation of cell wall metabolism in stress is thought to be responsible for decreased permeability and increased tolerance to antibiotics. The signaling systems that control cell wall metabolism under stress, however, are poorly understood. Here, we examine the cell wall regulatory function of a key cell wall regulator, the Serine Threonine Phosphatase PstP, in the model organism *Mycobacterium smegmatis.* We show that the peptidoglycan regulator CwlM is a substrate of PstP. We find that a phospho-mimetic mutation, *pstP* T171E, slows growth, mis-regulates both mycolic acid and peptidoglycan metabolism in different conditions, and interferes with antibiotic tolerance. These data suggest that phosphorylation on PstP affects its activity against various substrates and is important in the transition between growth and stasis.

Importance

Regulation of cell wall assembly is essential for bacterial survival and contributes to pathogenesis and antibiotic tolerance in mycobacteria, including pathogens such as *Mycobacterium tuberculosis*. However, little is known about how the cell wall is regulated in stress. We describe a pathway of cell wall modulation in *Mycobacterium smegmatis* through the only essential Ser/Thr phosphatase, PstP. We showed that phosphorylation on PstP is important in regulating

peptidoglycan metabolism in the transition to stasis and mycolic acid metabolism in growth. This regulation also affects antibiotic tolerance in growth and stasis. This work helps us to better understand the phosphorylation-mediated cell wall regulation circuitry in Mycobacteria.

Introduction

Tuberculosis (TB), an infectious disease caused by the bacterium *Mycobacterium tuberculosis* (*Mtb*) is one of the leading causes of death from infectious diseases (1). The fact that TB treatment requires at least a six month regimen with four antibiotics is partly due to the intrinsic antibiotic tolerance of *Mtb* (2, 3). Stressed *Mtb* cells can achieve a dormant or slow-growing state (4, 5) which exhibits antibiotic tolerance (6), cell wall thickening (7) and altered cell-wall staining (4).

The currently accepted cell wall structure of *Mtb* (8) is composed of three covalently linked layers (9): surrounding the plasma membrane, a peptidoglycan (PG) layer is covalently bound to an arabinogalactan layer. A lipid layer composed of mycolic acids surrounds the arabinogalactan layer, and the inner leaflet of this layer is covalently linked to the arabinogalactan (10). The outer leaflet of the mycolic acid layer contains free mycolic acids, trehalose mycolates and other lipids, glycolipids, glycans and proteins (11). The mycolic acid layer, or mycomembrane, is the outer membrane of mycobacteria and is the major contributor to impermeability of the cell wall (12-14).

In addition to serving as a permeability barrier, regulation of the cell wall likely contributes to antibiotic tolerance, either through further changes in permeability (15), or by changing the activity of antibiotic targets (16). Several studies have observed changes in the cell wall under stress (7, 15, 17, 18). These cell wall changes have been shown to correlate with increased antibiotic tolerance (19-21). This has led the prevalent model that stress-induced regulation of the cell wall contributes to antibiotic tolerance (22). While most of the extant data to support this model is correlative, we recently identified a mutant in *Msmeg* which specifically upregulates peptidoglycan metabolism in starvation and also causes decreased antibiotic tolerance in that condition (23). This shows that there is a causal relationship between cell wall regulation and antibiotic tolerance, at least in limited conditions in *Msmeg*.

Reversible protein phosphorylation is a key regulatory tool used by bacteria for environmental signal transduction to regulate cell growth (24-27). In *Mtb*, Serine/Threonine phosphorylation is important in cell wall regulation (28). *Mtb* has 11 Serine/Threonine Protein Kinases (STPKs) (PknA, PknB and PknD-L) and only one Serine/Threonine protein phosphatase (PstP) (29, 30).

Among the STPKs, PknA and PknB are essential for growth, and phosphorylate substrates many involved in cell growth and division (23, 31-34). Some of these substrates are enzymes whose activity is directly altered by phosphorylation. For example, all the enzymes in the FAS-II system of mycolic acid biosynthesis are inhibited by threonine phosphorylation (35-39). There are also cell wall regulators

that are not enzymes, but whose phosphorylation by STPKs affects cell shape and growth. For example, the regulator CwlM, once it is phosphorylated by PknB, activates MurA (23), the first enzyme in PG precursor biosynthesis (40). In the transition to starvation, CwlM is rapidly dephosphorylated in *Msmeg* (23). Mis-regulation of MurA activity increases sensitivity to antibiotics in early starvation (23), implying that phospho-regulation of CwlM promotes antibiotic tolerance. CwlM may also regulate other steps of PG synthesis (41). A recent phospho-proteomic study showed that transcriptional repression of the operon that contains both *pstP* and *pknB* leads to increased phosphorylation of CwlM (42). While the effects of the individual genes were not separated (42), this suggests that PstP could dephosphorylate CwlM.

PstP is essential in *Mtb* and *Msmeg* (43, 44). It is a member of the Protein phosphatase 2C (PP2C) subfamily of metal-dependent protein Serine/Threonine phosphatases (45) which strictly require divalent metal ions for activity (46, 47). PP2C phosphatases are involved in responding to environmental signals, regulating metabolic processes, sporulation, cell growth, division and stress response in a diverse range of prokaryotes and eukaryotes (48-53). $PstP_{Mtb}$ shares structural folds and conserved residues with the human PP2Cα (54), which serves as the representative of the PP2C family. $PstP_{Mtb}$ has an N-terminal cytoplasmic enzymatic domain, a transmembrane pass and a C-terminal extracellular domain (45).

Many of the proteins known to be dephosphorylated by PstP (35, 45, 55-58) are involved in cell wall metabolism; however, the effects of this activity seem to differ. For example, dephosphorylation of CwlM should decrease PG metabolism in stasis (23). But, dephosphorylation of the FAS-II enzymes (35-37, 59-61) should upregulate lipid metabolism in growth. However, PG and lipid metabolism are expected to be coordinated (22). Therefore, PstP must be able to alter substrate specificity in growth and stasis.

PstP$_{Mtb}$ is itself phosphorylated on Threonine residues 137, 141, 174 and 290 (55). We hypothesized that phosphorylation of the threonine residues of PstP might help coordinate activity against different substrates through changes in access to substrates, or through toggling catalytic activity against substrates.

We report here that phospho-ablative and phospho-mimetic mutations at the phospho-site T171 of PstP$_{Msmeg}$ (T174 in PstP$_{Mtb}$) alter growth rate, cell length, cell wall metabolism and antibiotic tolerance in *Msmeg*. Strains of *Msmeg* with *pstP* T171E alleles grow slowly, are unable to properly downregulate PG metabolism and upregulate antibiotic tolerance in the transition to starvation. We observed that the same mutation has nearly opposite effects on mycolic acid layer metabolism. We also report that PstP$_{Mtb}$ dephosphorylates CwlM$_{Mtb.}$

Materials and Methods

Bacterial strains and culture conditions

All *Mycobacterium smegmatis* mc^2155 ATCC 700084 cultures were started in 7H9 (Becton, Dickinson, Franklin Lakes, NJ) medium containing 5 g/liter bovine serum albumin (BSA), 2 g/liter dextrose, 0.003 g/liter catalase, 0.85 g/liter NaCl, 0.2% glycerol, and 0.05% Tween 80 and incubated at 37°C until log. phase. Hartmans-de Bont (HdB) minimal medium made as described previously (62) without glycerol was used for starvation assays. Serial dilutions of all CFU counts were plated on LB Lennox agar (Fisher BP1427-2).

E. coli Top10, XL1Blue and Dh5α were used for cloning and *E. coli* BL21 Codon Plus was used for protein expression. Antibiotic concentrations for *M. smegmatis* were 25 µg/ml kanamycin. 50 µg/ml hygromycin and 20 µg/ml zeocin. Antibiotic concentrations for *E. coli* were 50 µg/ml kanamycin, 25 µg/ml zeocin, 20 µg/ml chloramphenicol and 140 µg/ml ampicillin.

Strain construction

The $PstP_{Msmeg}$-knockdown strain was made first by creating a merodiploid strain and then by deleting the native $pstP_{Msmeg}$ gene from its chromosomal location. The merodiploid strain was generated by introducing a constitutively expressing

pstP$_{Mtb}$ gene cloned on an StrR plasmid at the L5 attB integration site. The *pstP*$_{Msmeg}$ gene (MSMEG_0033) at the native locus was then deleted by RecET-mediated double stranded recombineering approach using a 1.53 kb loxP-hyg-loxP fragment carrying a 125 bp regions flanking the *pstP*$_{Msmeg}$ gene, as described (63). The recombineering substrate was generated by two sequential overlapping PCR of the loxP-hyg-loxP substrate present in the plasmid pKM342. The downstream flanking primer used in the first PCR also carried an optimized mycobacterial ribosome binding site in front of the start codon of MSMEG_0032 to facilitate the expression of the genes present downstream of *pstP*$_{Msmeg}$ *in* the *Msmeg pstP-pknB* operon.

Deletion of the *pstP*$_{Msmeg}$ gene was confirmed by PCR amplification and sequencing of the 5' and 3' recombinant junctions, and the absence of an internal wild-type *pstP*$_{Msmeg}$ PCR product. The *pstP*$_{Mtb}$ allele present at the L5 site was then swapped, as described (64), with a tet-regulatable *pstP*$_{Mtb}$ allele (RevTetR-P750- *pstP*$_{Mtb}$-DAS tag-L5-Zeo plasmid). The loxP-flanked *hyg* marker present in the chromosomal locus was then removed by expressing Cre from pCre-sacB-Kan, and the Cre plasmid was subsequently cured from this strain by plating on sucrose. We named this strain CB1175.

Different alleles of *pstP* were attained by swapping the Wild-type (WT) allele at L5 site of CB1175 as described (65). In order to do so, the wild-type (WT) and the phosphoablative alleles of *pstP*$_{Msmeg}$ alleles were at first cloned individually

into a kanamycin resistant-marked L5 vector pCT94 under a TetO promoter to generate vectors pCB1206-1208 and pCB1210, which would swap out the zeocin-resistance marked vector at the L5 site in CB1175. The strong TetO promoter in the vectors pCB1206-1208 and pCB1210 was swapped with an intermediate strength promoter p766TetON6 (cloned from the vector pCB1030 (pGMCgS-TetON-6 sspB) to generate the L5 vectors pCB1282-85. pCB1285 was used as the parent vector later on to clone in the phosphomimetic *pstP*$_{Msmeg}$ alleles under p766TetON6.

These kanamycin resistance-marked vector constructs were then used to swap out the zeocin resistance-marked vector at the L5 site of CB1175 to attain different allelic strains of *pstP*$_{Msmeg}$ as described (65).

Growth Curve assay

At least three biological replicates of different *pstP*$_{Msmeg}$ allele strains were grown in 7H9 media up to log. phase. The growth curves were performed in non-treated 96 well plate using plate reader (BioTek Synergy neo2 multi mode reader) in 200µl 7H9 media starting at OD_{600}=0.1. Exponential growth equation was used to calculate the doubling times of each strain using the least squared ordinary fit method in GraphPad Prism (Version 7.0d). P values were calculated using two-tailed, unpaired t-tests.

Cell staining

For staining cells in log. phase, 100µl culture in 7H9 was incubated at 37°C with 1µl of 10mM DMN-Tre for 30 minutes and 1µl of 10mM HADA for 15 minutes. Cells were then pelleted and resuspended in 1x phosphate buffered saline (PBS) supplemented with 0.05% Tween 80 and fixed with 10µl of 16% paraformaldehyde (PFA) for 10 minutes at room temperature. Cells were then washed and resuspended in PBS + Tween 80.

For starvation microscopy, cultures were shaken for 4 hours in HdB media without glycerol at 37°C. 500µl of each culture were pelleted and concentrated to 100µl, then incubated at 37°C with 1µl of 10mM DMN-Tre for 1 hour and 3µl of 10mM HADA for 30 minutes. Cells were then washed and fixed as above. The total time of starvation before fixation was 5.5 hours.

Microscopy and Image Analysis

Cells were imaged with a Nikon Ti-2 widefield epifluorescence microscope with a Photometrics Prime 95B camera and a Plan Apo 100x, 1.45 NA objective lens. The green fluorescence images for DMN-Tre staining were taken with a 470/40nm excitation filter and a 525/50nm emission filter. Blue fluorescence images for HADA staining were taken using 350/50nm excitation filter and 460/50nm emission filter. All images were captured using NIS Elements software

and analyzed using FIJI and MicrobeJ (66). For cell detection in MicrobeJ, appropriate parameters for length, width and area were set. The V-snapping cells were split at the septum so that each daughter cell could be considered as a single cell. Any overlapping cells were excluded from analysis.

Length and mean-intensities of HADA and DMN-Tre signals of 300 cells from each strain (100 cells per replicate) were quantified using MicrobeJ. The values of the mean intensities of 300 cells of each strain are represented in the graph as percentages of the highest mean intensity from all the cells in that experiment. An unpaired, two-tailed t-test was performed on the means of the 300 percentage-intensity values of each strain.

Western Blots

Cultures were grown in 7H9 to OD_{600}=0.8 in 10ml 7H9 media, pelleted and resuspended in 500µL PBS with 1mM PMSF and lysed (MiniBeadBeater-16, Model 607, Biospec). Supernatants from the cell lysate were run on 12% resolving Tris-Glycine gels and then transferred onto PVDF membrane (GE Healthcare). Rabbit α-strep antibody (1:1000, Abcam, ab76949) in TBST buffer with 0.5% milk and goat α-rabbit IgG (H+L) HRP conjugated secondary antibody (1:10,000, ThermoFisher Scientific 31460) in TBST were used to detect PstP-strep. For starvation experiments, cultures were first grown to log. phase, then starved in HdB no glycerol media starting at OD=0.5 for 1.5 hour.

For Western blots of *in vitro* assays, samples were run on 12% SDS gel (Mini-Protean TGX, Biorad, 4561046) and then transferred onto PVDF membrane (GE Healthcare). Mouse α-His antibody (1:1000, Genscript A00186) in TBST buffer with 0.5% BSA and goat α-mouse IgG (H+L) HRP conjugated secondary antibody (1:10,000, Invitrogen A28177) were used to detect His-tagged proteins on the blot. The blots were stripped (Thermo Scientific, 21059) and re-probed with Rabbit α-Phospho-Threonine antibody (1:1000, Cell Signaling #9381) and goat α-rabbit IgG (H+L) HRP conjugated secondary antibody (1:10,000, ThermoFisher Scientific 31460) to detect phosphorylation on the blots.

Antibiotic assays

For antibiotic assays in log. phase, log. phase cultures were diluted in 7H9 media to OD600= 0.05 before treatment. For starvation assays, cells were grown to OD_{600}=0.5, pelleted, washed and resuspended in HdB starvation (with no glycerol and 0.05% Tween) media at OD_{600}=0.3 and incubated at 37°C for a total of 5.5 hours. The cultures were then diluted to OD_{600}=0.05 before antibiotic treatment. 8 µg/ml and 45 µg/ml meropenem was used for log. phase and starved cultures, respectively. 10 µg/ml and 90 µg/ml isoniazid was added to log. phase and starved cultures, respectively. 100 µg/ml and 900 µg/ml D-cycloserine was used for log. phase and starved cultures, respectively. 50 µg/ml and 360 µg/ml trimethoprim was added to log. phase and starved cultures, respectively. Samples from the culture were serially diluted and plated on LB agar before and

after treatment, and colony forming units were calculated.

Protein Purification

All the proteins were expressed using *E. coli* BL21 Codon Plus cells. N-terminally his-MBP tagged $PknB_{Mtb}$ was expressed and purified as described (67). His-$PstP_cWT_{Mtb}$ (1-300 amino acids of the cytosolic domain, (68)) and His-SUMO-$CwlM_{Mtb}$ were both expressed overnight by IPTG induction (1mM and 1.3mM, respectively), purified on Ni-NTA resin (G-Biosciences, #786-940 in 5 ml Bio-Scale™ Mini Cartridges, BioRad #7324661), then dialyzed, concentrated and run over size exclusion resin (GE Biosciences Sephacryl S-200 in HiPrep 26/70 column) to obtain soluble proteins. The buffer for His-SUMO-$CwlM_{Mtb}$ was 50mM Tris pH 8, 350mM NaCl, 1mM DTT and 10% glycerol. The buffer for His-$PstP_cWT_{Mtb}$ was 50mM Tris pH 7.5, 350mM NaCl, 1mM DTT and 10% glycerol. 20mM imidazole was added to each buffer for lysis and application to the Ni-NTA column, and 250mM imidazole was added for elution. His-$PstP_cT174E_{Mtb}$ was expressed and purified using the same conditions and buffers used for His-$PstP_cWT_{Mtb}$.

In vitro Dephosphorylation assay

Purified His-SUMO-$CwlM_{Mtb}$ was phosphorylated with the purified kinase His-MBP-$PknB_{Mtb}$ for 1 hour at room temperature in presence of 0.5mM ATP, 1mM

300 $MnCl_2$ and buffer (50mM Tris pH 7.5, 250mM NaCl, and 1mM DTT). The amount
301 of kinase was one-tenth of the amount of substrate in the phosphorylation
302 reaction. To stop the kinase reaction by depleting ATP, 0.434 units of calf
303 intestinal alkaline phosphatase (Quick CIP, NEB, MO525S) per µg of His-SUMO-
304 $CwlM_{Mtb}$ was added to the reaction mixture and incubated for 1 hour at 37°C. The
305 reaction mixture was then divided into five parts for the different phosphatase
306 samples and a control with buffer.
307
308 Two individually expressed and purified batches of both His-$PstP_cWT_{Mtb}$ and His-
309 $PstP_cT1714E_{Mtb}$ were used as biological replicates to perform the
310 dephosphorylation assay. The reaction was carried out at room temperature for
311 up to 90 minutes in presence of phosphatase buffer (50mM Tris pH 7.5, 10mM
312 $MnCl_2$, and 1mM DTT). The amount of phosphatase used was half the amount of
313 His-SUMO-$CwlM_{Mtb}$.
314
315 The intensities of the α-His and the α-Phospho-Threonine signals on the blots
316 were quantified with FIJI. The intensities of the α-His and the α-Phospho-
317 Threonine signals at each time-point were normalized against the respective
318 antibody-signal intensity at 0m. These relative intensities were used to calculate
319 α-Phospho-Threonine/α-His for each time-point and the values were plotted over
320 time using GraphPad Prism (version 7.0d).
321
322

Results

Phospho-site T171 of PstP$_{Msmeg}$ impacts growth rate

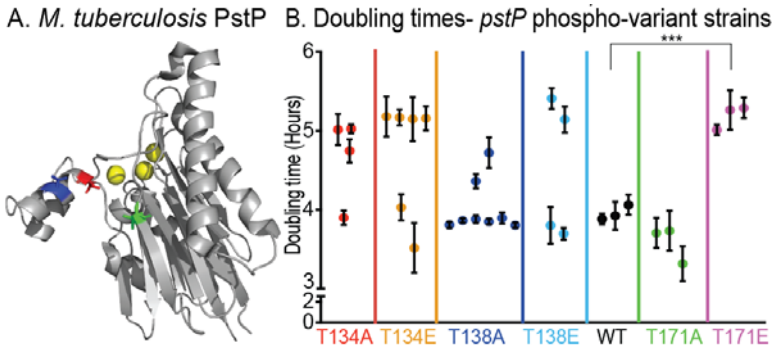

FIG 1. Phospho-site T171 on PstP affects growth.

(A) Crystal structure of PstP from *M. tuberculosis (*PstP$_{Mtb}$) (54). The threonine (T) sites on PstP$_{Mtb}$ phosphorylated by the kinases PknA and PknB (55) are highlighted on the structure: red- PstP$_{Mtb}$ T137 (T134 in PstP$_{Msmeg}$), blue- PstP$_{Mtb}$ T141 (T138 in PstP$_{Msmeg}$) and green- PstP$_{Mtb}$ T174 (T171 in PstP$_{Msmeg}$).

B) Doubling times of strains containing *pstP*$_{Msmeg}$WT, phospho-ablative mutant alleles *pstP*$_{Msmeg}$ T134A, T138A and T171A and phospho-mimetic mutant alleles *pstP*$_{Msmeg}$ T134E, T138E and T171E. Each dot is the mean of doubling times from two to three different experiments on different dates of a single isolated clone. The error bars represent the standard deviation. P value= 0.0009.

PstP is necessary for cell growth in *Msmeg* (42, 43) and phosphorylation increases PstP$_{Mtb}$'s activity against small molecule substrates *in vitro* (42, 43, 55). To see if the phosphorylations on PstP regulate cell growth, we made *Msmeg*

343 strains with either phospho-ablative (T>A) or phospho-mimetic (T>E) alleles (69)
344 at each of the three conserved phosphorylation sites of $PstP_{Mtb}$ (42, 43, 55) (Fig.
345 1A) and performed growth curves. We found that biological replicates of the
346 T134A, T134E, T138A and T138E mutant strains had bi-modal distributions of
347 doubling times (Fig. 1B). Phospho-sites T134 and T138 in $PstP_{Mtb}$ map to the flap
348 subdomain (54) (Fig. 1A). This subdomain varies greatly in sequence and
349 structure across different PP2C family members and has been shown to be
350 important in regulating substrate binding, specificity and catalytic activity (54, 70-
351 72). Particularly, T138A and T138E variants of the serine threonine phosphatase
352 tPphA from *Thermosynechococcus elongatus* showed differences in substrate
353 reactivity (70). This suggests that phosphorylation at T134 and T138 could be
354 very important in regulating the normal activity of $PstP_{Msmeg}$ in the cell. We think
355 that the inconsistent doubling times of those strains result may result from the
356 formation of suppressor mutants, which we will study in future work.
357 The *Msmeg* strains with *pstP* T171A and T171E mutations showed consistent
358 and reproducible growth rates (Fig. 1B). The T171A mutants showed no
359 significant difference in doubling time compared to the wild-type, but the T171E
360 grew more slowly than the wild-type. Since T171E mimics constitutive
361 phosphorylation, this result suggests that the continuous presence of a
362 phosphate on T171 downregulates or interferes with cell growth.
363
364
365

366 **PstP$_{Mtb}$ WT and PstP$_{Mtb}$ T174E dephosphorylate CwlM$_{Mtb}$ *in vitro.***

367 Only a few substrates of PstP have been biochemically verified: some STPKs
368 including PknA and PknB, (45, 55, 57, 58), KasA and KasB (35, 55, 57), and
369 EmbR (56). The STPK PknB phosphorylates CwlM, which is an activator of PG
370 biosynthesis (23). CwlM is rapidly dephosphorylated in the transition to starvation
371 in *Msmeg* (23), and becomes hyper-phosphorylated when PstP is depleted in
372 *Msmeg* (42) which suggests PstP dephosphorylates CwlM.

373

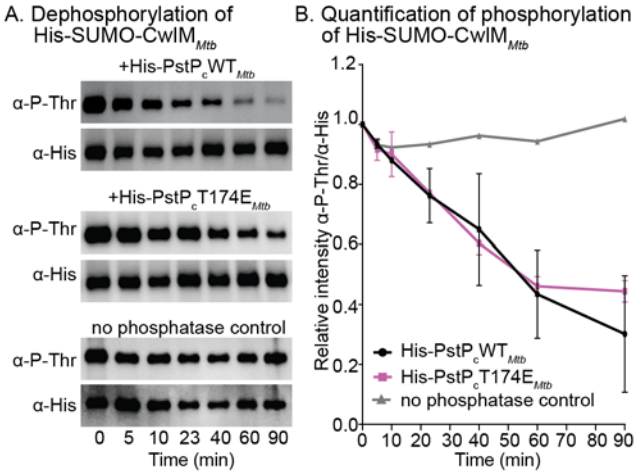

374

375 **FIG 2 PstP$_{Mtb}$ dephosphorylates CwlM$_{Mtb}$.**

376 (A) α-P-Thr and α-His Western blots of *in vitro* phosphatase reactions with His-
377 PstP$_c$WT$_{Mtb}$ (top panel) and His-PstP$_c$T174E$_{Mtb}$ (middle panel), and no phosphatase
378 control (bottom panel) and phosphorylated His-SUMO-CwlM$_{Mtb}$. Assay was performed at
379 least twice with two individually purified batches of each phosphatase, one set of images
380 is shown here.

381 (B) Quantification of relative intensities of α-P-Thr over α-His on Western blots. P values
382 were calculated using two-tailed unpaired t-test. All the P values of WT vs T171E at any
383 given time were non-significant. P values of WT vs T171E at 5min = 0.682669, 10min-

384 0.809025, 23min= 0.933929, 40min= 0.831124, 60min= 0.876487 and 90min=
385 0.545030. The error bars represent standard error of means.
386
387 To test whether PstP and its T174 (T171 in *Msmeg)* phospho-mimetic variant
388 directly dephosphorylate CwlM, we performed an in *vitro* biochemical assay with
389 purified *Mtb* proteins. We purified His-MBP-PknB$_{Mtb}$, His-SUMO-CwlM$_{Mtb}$ and the
390 cytoplasmic region of PstP$_{Mtb}$ that has the catalytic domain (His-PstP$_c$WT$_{Mtb}$ or
391 PstP$_c$T174E$_{Mtb}$). PstP dephosphorylates itself rapidly (55), so the purified form is
392 unphosphorylated. We phosphorylated His-SUMO-CwlM$_{Mtb}$ by His-MBP-PknB$_{Mtb}$,
393 stopped the phosphorylation reaction with Calf Intestinal Phosphatase, and then
394 added His-PstP$_c$WT$_{Mtb}$ or PstP$_c$T174E$_{Mtb}$ to His-SUMO-CwlM$_{Mtb}$~P. Our control
395 assay with His-SUMO-CwlM~P without PstP$_c$WT$_{Mtb}$ or PstP$_c$T174E$_{Mtb}$ showed
396 that the phosphorylation on the substrate is stable (Fig. 2A, bottom panel). The
397 phosphorylation signal on His-SUMO-CwlM$_{Mtb}$ started decreasing within 5
398 minutes after addition of His-PstP$_c$WT$_{Mtb}$ and kept decreasing over a period of 90
399 minutes (Fig. 2A, top panel). This is direct biochemical evidence that the PG-
400 regulator CwlM$_{Mtb}$ is a substrate of PstP$_{Mtb.}$ We observed that the WT and T174
401 phospho-mimetic forms of PstP$_{Mtb}$ have no significant differences in activity
402 against His-SUMO-CwlM$_{Mtb}$~P *in vitro* (Fig. 2B).
403
404 These data show that, *in vitro,* the activity of the catalytic domain of PstP against
405 a single substrate is not affected by a negative charge on T171$_{Msmeg}$/T174$_{Mtb}$. The
406 phenotypes of the full-length *pstP* T171 phospho-alleles (Fig. 1B, 3, 4 and 5)

indicate that this *in vitro* data do not reflect the full complexity of PstP's regulation *in vivo*.

Phospho-site T171 of PstP$_{Msmeg}$ regulates cell length

To assess how the phospho-site T171 affects growth, we examined the cell morphology of *pstP* T171 mutants and wild-type (Fig. 3A and B). The quantification of cell length revealed that the *pstP* T171A cells were shorter (mean=4.0261 ± 0.0755) in log. phase than the wild-type cells (mean= 4.5027 ± 0.0704) (Fig. 3A). The *pstP* T171E strain has cell lengths similar to the wild-type (difference between means= 0.05294 ± 0.1163) (Fig. 3A and B) despite the slower growth (difference between means= -1.037 ± 0.1161) (Fig. 1B) in log. phase.

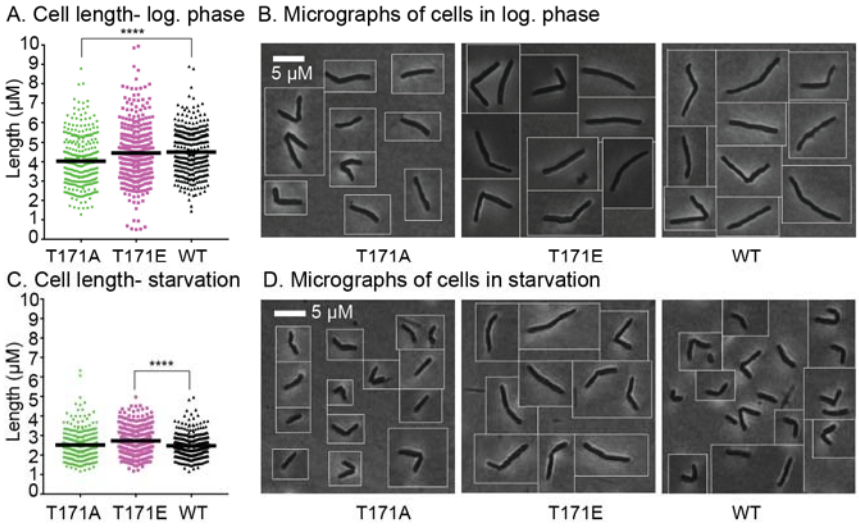

FIG 3. Phospho-site T171 on PstP$_{Msmeg}$ is important in regulating cell length.

(A) Quantification of cell lengths of isogenic *pstP* allele strains (WT, T17A and T171E) grown in 7H9 in log. phase. 100 cells from each of three biological replicates were measured. P values were calculated by unpaired t-test. P value = 0.000005.

(B) Representative phase images of cells from (A).

(C) Quantification of cell lengths of isogenic *pstP* allele strains (WT, T17A and T171E) after starvation in HdB with no glycerol for five and a half hours. 100 cells from each of three biological replicates were measured. P values were calculated by unpaired t-test. P value= 0.000003.

(D) Representative phase images of cells from (C).

PstP could promote the transition from growth to stasis by downregulating the activity of some cell growth substrates, such as CwlM, PknA or PknB, which all promote growth when phosphorylated (23, 42, 45, 55, 58). PstP likely has dozens of other substrates which may be regulated similarly (23, 42, 45, 55, 58). To test if phospho-site T171 of $PstP_{Msmeg}$ affects the transition to stasis, we transferred the strains from log. phase to minimal HdB media with Tween 80 as the only source of carbon, which leads *Msmeg* cells to reductively divide (73). We aerated the cultures for 5.5 hours before imaging (Fig. 3C and D). The effects of phospho-mutations of $PstP_{Msmeg}$ on starved cells were the inverse of what we saw in the log. phase. $pstP_{Msmeg}$ T171E cells in starvation were longer than the wild-type and T171A, and looked like log. phase cells. These data imply that phosphorylation on T171 of $PstP_{Msmeg}$ is involved in cell size regulation upon carbon starvation.

Phospho-site T171 of $PstP_{Msmeg}$ regulates cell wall metabolism

Since $pstP_{Msmeg}$ T171 seems to play a role in regulating cell length in growth and stasis, we hypothesized that it affects cell wall metabolism in different phases. To

448 test this, we used fluorescent dyes that preferentially stain metabolically active
449 cell wall(74, 75). We stained T171 allele variant cells from log. phase and after
450 5.5 hours of carbon starvation with both the fluorescent D-amino acid HADA,
451 which is incorporated into the PG, (74, 76, 77) (Fig. 4A and C, and Fig. S1A and
452 B) and the fluorescent trehalose DMN-Tre, which stains the mycomembrane (75)
453 (Fig. 4B and D, and Fig. S1A and B).

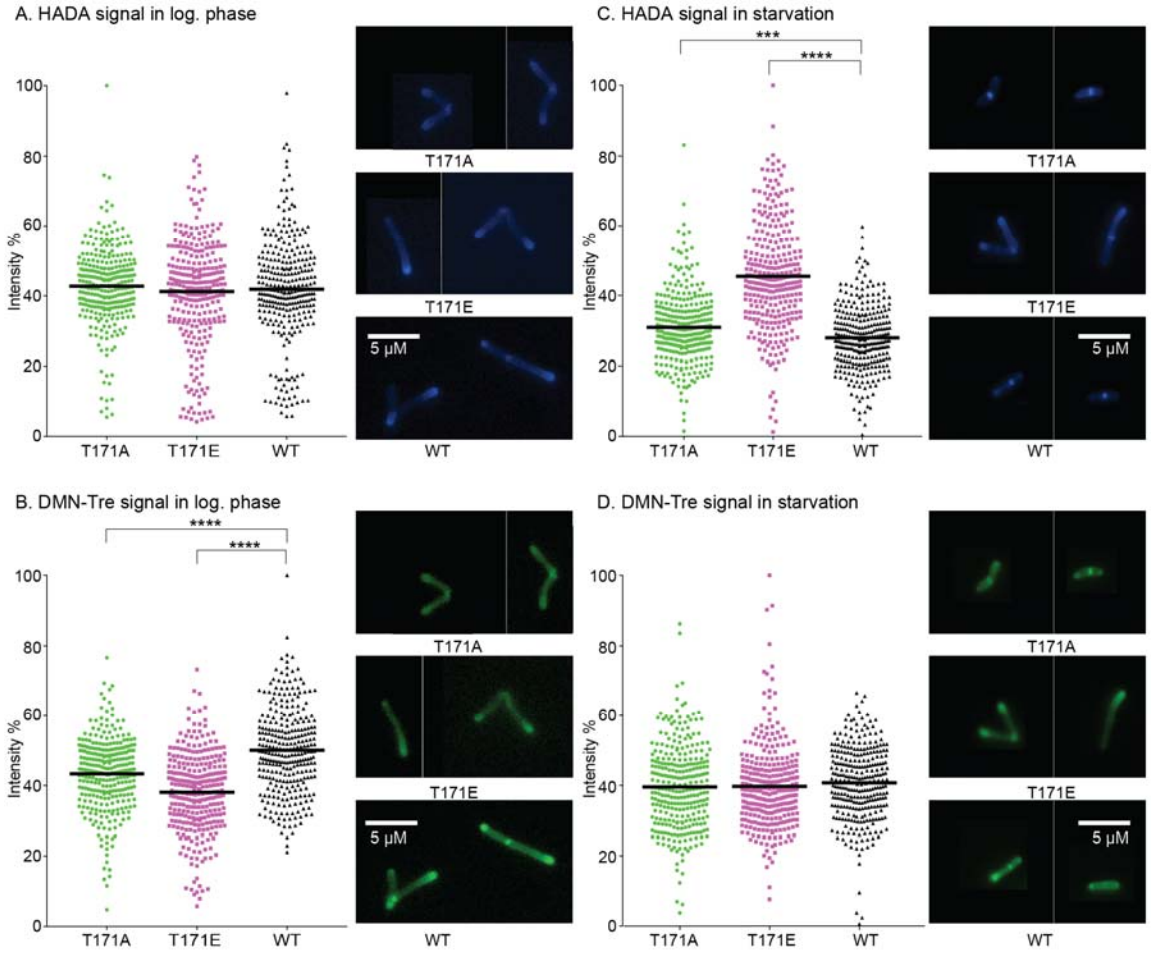

454

455 **FIG 4. Phospho-site T171 of PstP alters cell wall staining.**

456 (A) and (B) Quantification of mean intensities of HADA (A) and DMN-Tre (B) signals of
457 *pstP* allele strains (WT, T17A and T171E) in log. phase cells. P values of both WT vs.
458 T171A and WT vs. T171E= 0.000001.

(C) and (D) Quantification of mean intensities of HADA (C) and DMN-Tre (D) signals of starved *pstP* allele strains (WT, T17A and T171E) after 5.5 hours in HdB with no glycerol. P value of WT vs. T171A= 0.0002 and WT vs. T171E = 0.000001.
For all experiments, mean intensities of signals from 100 cells from each of three biological replicates of every strain were measured using MicrobeJ. The values of the mean intensities are represented in percentages of the maximum value of all intensities for all strains. P values were calculated by a two-tailed, unpaired t-test.

The PG staining intensity between the strains was the same in log. phase (Fig. 4A). In starvation, the *pstP*$_{Msmeg}$ T171E mutant stained much more brightly with HADA than the other strains (Fig. 4C). This suggests that phosphorylation on PstP$_{Msmeg}$ T171 may inhibit the downregulation of PG layer biosynthesis in the transition to stasis, but that this phospho-site is not important in modulating PG metabolism during rapid growth.

Staining with DMN-Tre, which correlates with assembly of the trehalose mycolate leaflet of the mycomembrane (75), shows the inverse pattern. The strains stain similarly in starvation (Fig. 4D). In log. phase, however, both mutants show a significant decrease in DMN-Tre signal compared to the wild-type (Fig. 4B), although the *pstP*$_{Msmeg}$ T171E mutant has the weakest staining. DMN-Tre is incorporated via Ag85-mediated trehalose mycolate metabolism of the mycomembrane (75). Its fluorescence is sensitive to the hydrophobicity of the membrane and to changes in cytoplasmic mycolic acid metabolism (75).

Our data in Fig. 4A and C suggest that phosphorylation on PstP$_{Msmeg}$ T171 impacts PG layer metabolism in starvation, but not growth. But the same phosphorylation appears to regulate the trehalose mycolate metabolism in growth, but not starvation (Fig. 4B and D).

Phospho-site T171 of PstP$_{Msmeg}$ affects antibiotic tolerance

Stresses that arrest cell growth in mycobacteria are associated with increased antibiotic tolerance (15, 18, 78-80). We hypothesized that if *Msmeg* fails to downregulate PG synthesis in starvation, (Fig. 4C), then it might be more susceptible to a PG targeting drug. We treated *pstP*$_{Msmeg}$ wild-type, T171A and T171E strains in log. phase and starvation with meropenem, which targets the cross-linking in the PG cell wall (81), and quantified survival by CFU. We saw that the *pstP*$_{Msmeg}$ T171E strain was more susceptible in starvation, compared to *pstP*$_{Msmeg}$ T171A and wild-type strains (Fig. 5B), but survived similarly in log. phase, except at very late time points when it was more tolerant.

We also treated *pstP*$_{Msmeg}$ wild-type, T171A and T171E strains in log. phase and starvation with D-cycloserine, which inhibits incorporation of D-alanine into PG pentapeptides in the cytoplasm (82, 83). The results were similar to those in meropenem: the strains survived similarly in log. phase (Fig. 5C), but the *pstP*$_{Msmeg}$ T171E strain was more sensitive in starvation (Fig. 5D). The apparent failure of the *pstP*$_{Msmeg}$ T171E strain to downregulate PG synthesis (Fig. 4C)

505 likely makes it more sensitive to both the PG inhibitors in starvation (Fig. 5B and

506 D).

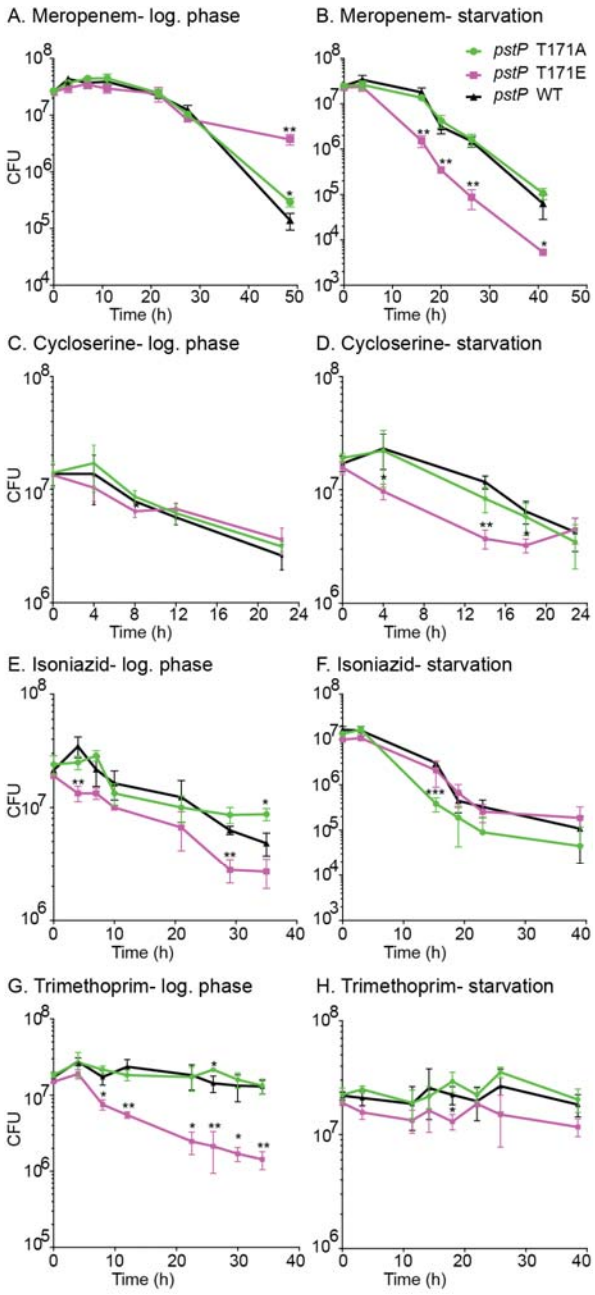

507

508 **FIG 5 Phospho-site T171 of PstP plays a role in antibiotic sensitivity.**

509 Survival of *pstP* allele strains (WT, T17A and T171E) in different media and antibiotics.

510 (A) In 7H9, treated with 8µg/ml of meropenem. P values of WT vs. T171E at 3h=

511 0.043024, WT vs. T171A at 48.5h= 0.001487 and WT vs. T171E at 48.5h = 0.018144.

(B) In HdB (no glycerol, 0.05% Tween) for 5.5 hours, then treated with 45µg/ml of meropenem. P values of WT vs. T171E at 16h= 0.002876, 23h=0.006978, 26.3h= 0.003679 and 41h= =0.045922.

(C) In 7H9, treated with 100µg/ml of D-cycloserine. P values of WT vs. T171E at 8h= 0.032189.

(D) In HdB (no Glycerol, 0.05% Tween) for 5.5 hours, then treated with 900µg/ml of D-cycloserine. P values of WT vs. T171E at 3.5h= 0.046062, 14h= 0.001198 and 18h= 0.022088.

(E) In 7H9, treated with 10µg/ml of isoniazid. P values of WT vs. T171E at 4h=0.007995, WT vs. T171E at 29h= 0.001978 and WT vs. T171A at 35h= 0.052499.

(F) In HdB (no Glycerol, 0.05% Tween) for 5.5 hours, then treated with 90µg/ml of isoniazid. P values of WT vs. T171A at 15.3h=0.000848.

(G) In 7H9, treated with 50µg/ml of trimethoprim. P values of WT vs. T171E at 4h= 0.022646, 8h= 0.012762, 12h= 0.005294, 22.5h= 0.014885, 26h= 0.004690, 30h= 0.017293 and 34h= 0.001694.

(H) In HdB (no Glycerol, 0.05% Tween) for 5.5 hours, then treated with 360µg/ml of trimethoprim. P values of WT vs. T171A at 18h= 0.023064. All experiments were done at least twice, and representative data are shown. All P values were calculated using two-tailed, unpaired t-test. All error bars represent standard deviation (SD).

Next, we treated our wild-type and *pstP*$_{Msmeg}$ T171 mutant strains with isoniazid, which targets InhA in the FAS-II pathway of mycolic acid synthesis (84). We do not see significant differences in isoniazid sensitivity between the strains in starvation (Fig. 5F). In log. phase, we see that the *pstP*$_{Msmeg}$ T171E strain is more susceptible to isoniazid than the *pstP*$_{Msmeg}$ T171A and the wild-type strains

537 (Fig. 5E). Our data (Fig. 5E) suggest that phosphorylation on PstP$_{Msmeg}$ T171
538 mis-regulates the mycolic acid biosynthesis pathway of mycomembrane
539 metabolism (Fig. 4C), thus increasing isoniazid susceptibility.
540
541 To see if the PstP T171 phospho-site affects susceptibility to a drug that does not
542 target the cell wall, we treated the strains with trimethoprim, which targets
543 thymidine biosynthesis in the cytoplasm (85). We see that, in log. phase, *pstP*
544 T171E is very susceptible to this drug (Fig. 5G), while the wild-type and T171A
545 strains are tolerant. All strains were tolerant to trimethoprim in starvation (Fig.
546 5H). This shows that mis-regulation of PstP may impact processes beyond cell
547 wall metabolism affecting antibiotic tolerance in turn.
548
549 Trimethoprim is a hydrophobic drug which is taken up via passive diffusion (86).
550 Therefore, permeability to trimethoprim is expected to be affected by changes in
551 mycomembrane metabolism in log. phase (Fig. 4C and 5E). It is notable that
552 *pstP* phospho-allele strains in starvation do not exhibit differences in DMN-Tre
553 staining (Fig. 4D) or isoniazid (Fig. 5F) or trimethoprim sensitivity (Fig. 5H), which
554 suggests that susceptibility to trimethoprim, could be determined largely by
555 permeability of the mycomembrane layer. D-cycloserine, on the other hand, is
556 hydrophilic and therefore its uptake is likely dependent on porins (87, 88), and
557 therefore less sensitive to changes in the mycomembrane. So, sensitivity to D-
558 cycloserine (Fig. 5C and D) appears to be largely dependent on regulation of PG
559 metabolism (Fig. 4A and C).

Our data show that phospho-site T171 of PstP regulates mycolic acid layer biosynthesis in growth, and PG layer metabolism in starvation. Mis-regulation of PstP can increase sensitivity to cell wall targeting drugs in both growth and stasis.

Discussion

Previous studies on mycobacterial phospho-regulation suggest that PstP could play a critical role in modulating cell wall metabolism in the transition between growth and stasis (18, 22, 23, 35, 42, 55, 58, 89). In this work, we explored how the phosphorylation of PstP contributes to this regulation. We report here that the phospho-site T171 of $PstP_{Msmeg}$ impacts growth, cell wall metabolism and antibiotic tolerance. We found that the PG master regulator $CwlM_{Mtb}$ is a substrate of $PstP_{Mtb}$. Our findings indicate that the phosphorylation on PstP affects PG metabolism in stasis and the mycolic acid metabolism during growth.

PG is regulated by phosphorylation factors at several points along the biosynthesis pathway (23, 41, 67, 90), mostly by PknB. PknB's kinase activity is responsive to lipid II that it detects in the periplasm (91). PstP is a global negative regulator of STPK phosphorylation (42) and has been proposed to be the cognate phosphatase of PknB in regulating cell growth (22, 42, 58, 92). Our data suggest that mutations at T171 of PstP do not affect PG metabolism in growth (Fig. 4A), but that the $PstP_{Msmeg}$ T171E strain fails to downregulate PG in starvation (Fig. 4C). We expect that PstP's activity against the PG regulator

583 CwlM (Fig 2A, top panel) should be critical for this downregulation because it
584 should de-activate MurA, the first enzyme in PG precursor synthesis (23, 40).
585
586 The *in vitro* biochemistry (Fig. 2A and B) predicts the log. phase staining data
587 (Fig. 4A), where the *pstP* T171E variant has no difference in apparent PG
588 activity. The proximity of a phospho-site to the substrate binding site of an
589 enzyme may affect the catalytic activity directly (93) but T174 maps to the β-
590 sheet core (β8) in $PstP_{Mtb}$, which is distant from the active site (Fig. 1A) (54). The
591 PG staining in starvation suggests that the $PstP_{Msmeg}$ T171E phospho-mimetic
592 variant might dephosphorylate CwlM more slowly *in vivo* (Fig. 5B), but this is not
593 what we see *in vitro* (Fig. 2A and B). Therefore, it is possible that, in starvation,
594 phosphorylation at this site may affect PstP's interaction (94) with other
595 regulatory proteins (95-97) that could modulate PstP's activity against PG
596 substrates, or it could affect access to substrates via localization changes.
597
598 Synthesis of the various mycobacterial cell wall layers are likely synchronized
599 (22, 98). PknB almost surely plays a crucial role in connecting PG and mycolic
600 acid metabolism during growth. If PG metabolism is slowed, PknB could sense
601 the accumulation of periplasmic lipid II (91) and signal to halt mycolic acid
602 biosynthesis by inactivating the FAS-II enzymes and the trehalose monomycolate
603 transporter MmpL3 (92) via phosphorylation (35-37, 59-61, 92). Our data imply
604 that PstP helps balance the effects of these inhibitory phosphorylations to allow
605 coordinated synthesis of mycolic acids in log. phase (Fig. 4B and 5E). Mis-

606 phosphorylation of PstP likely disrupts this coordination and seems to decrease
607 mycolic acid layer metabolism. This may partly explain the slow growth of the
608 *pstP* T171E mutants (Fig. 1B).
609
610 We propose that PstP's regulation of mycolic acid layer biosynthesis occurs in
611 the cytoplasm. DMN-Tre incorporation into the mycomembrane is directly
612 catalyzed by secreted Ag85 enzymes (75, 99), but it is indirectly affected by both
613 cytoplasmic changes in mycolic acid synthesis (75) and altered mycomembrane
614 hydrophobicity (100). PstP and all the STPKs work in the cytoplasm, and there
615 are currently no known systems whereby secreted proteins like Ag85 can be
616 regulated by phosphorylation. All the enzymes of the FAS-II complex, which
617 elongates fatty acids into the long lipids used in mycolic acids (84), are
618 downregulated by phosphorylation (35-37, 59-61), and two are biochemically
619 verified substrates of PstP (35). MmpL3, the mycolic acid flippase (101), is also
620 inhibited by phosphorylation (92). It is likely that PstP could affect the activity of
621 the entire FAS-II complex, including the target of isoniazid, InhA, which is
622 inactivated by threonine phosphorylation (37, 60). Isoniazid is a small hydrophilic
623 drug and undergoes active diffusion via the porins (88, 102); therefore,
624 alterations in mycomembrane permeability are not likely to contribute
625 substantially to differences in isoniazid sensitivity. Although our data (Fig. 5E)
626 does not reveal the exact mis-regulated spot in the mycolic acid synthesis and
627 transport pathway, the higher susceptibility of the phosphomimetic strain (Fig.
628 5E) to isoniazid suggests that this metabolic pathway is affected. Our DMN-tre

staining also suggests that there should be a balance of non-phospho and phospho-form of $PstP_{Msmeg}$ T171 (Fig. 4B) during growth to regulate mycomembrane biosynthesis.

PstP may dephosphorylate the cell wall substrates directly, and/ or by de-activating their kinases (103) in both the PG and mycolic acid biosynthesis pathways. All these data combined suggest a complex cross-talk of the STPKs and PstP to regulate diverse cell wall substrates.

Acknowledgment

This work was supported by grants 1R15GM131317-01 and R01AI148917-01A1 to CCB from the National Institutes of Health, and by startup funds from the University of Texas at Arlington. We thank Kenan Murphy for the plasmids pDE54MCZD and pKM55 and Dirk Schnappinger for pDE43-MCS and RevTetR promoter plasmids used in this study.

682 **References:**

683 1. **World Health Organization**. 2019. Global Tuberculosis Report 2019.

684 2. **Nguyen L**. 2016. Antibiotic resistance mechanisms in M. tuberculosis: an
685 update. Arch Toxicol **90**:1585–1604.

686 3. **Jarlier V**, **Nikaido H**. 1994. Mycobacterial cell wall: structure and role in
687 natural resistance to antibiotics. **123**:11–18.

688 4. **Seiler P**, **Ulrichs T**, **Bandermann S**, **Pradl L**, **Jörg S**, **Krenn V**,
689 **Morawietz L**, **Kaufmann SHE**, **Aichele P**. 2003. Cell-wall alterations as
690 an attribute of Mycobacterium tuberculosis in latent infection. J Infect Dis
691 **188**:1326–1331.

692 5. **Muñoz-Elías EJ**, **Timm J**, **Botha T**, **Chan WT**, **Gomez JE**, **McKinney**
693 **JD**. 2004. Replication Dynamics of Mycobacterium tuberculosis in
694 Chronically Infected Mice. Infection and immunity **73**:546–551.

695 6. **Wallis RS**, **Patil S**, **Cheon SH**, **Edmonds K**, **Phillips M**, **Perkins MD**,
696 **Joloba M**, **Namale A**, **Johnson JL**, **Teixeira L**, **Dietze R**, **Siddiqi S**,
697 **Mugerwa RD**, **Eisenach K**, **Ellner JJ**. 1999. Drug tolerance in
698 Mycobacterium tuberculosis. Antimicrobial Agents and Chemotherapy
699 **43**:2600–2606.

700 7. **Cunningham AF**, **Spreadbury CL**. 1998. Mycobacterial stationary phase
701 induced by low oxygen tension: cell wall thickening and localization of the
702 16-kilodalton alpha-crystallin homolog. J Bacteriol **180**:801–808.

703 8. **Brennan PJ**. 2003. Structure, function, and biogenesis of the cell wall of
704 Mycobacterium tuberculosis. Tuberculosis **83**:91–97.

705 9. **Minnikin DE**. 1991. Chemical principles in the organization of lipid
706 components in the mycobacterial cell envelope. Research in
707 Microbiologoy **142**:423–427.

708 10. **Kieser KJ**, **Rubin EJ**. 2014. How sisters grow apart: mycobacterial
709 growth and division. Nat Rev Microbiology **12**:550–562.

710 11. **Marrakchi H**, **Lanéelle M-A**, **Daffé M**. 2014. Mycolic Acids: Structures,
711 Biosynthesis, and Beyond. Chemistry & Biology **21**:67–85.

712 12. **Hett EC**, **Rubin EJ**. 2008. Bacterial growth and cell division: a
713 mycobacterial perspective. Microbiology and Molecular Biology Reviews
714 **72**:126–156.

715 13. **Hoffmann C**, **Leis A**, **Niederweis M**, **Plitzko JM**, **Engelhardt H**. 2008.
716 Disclosure of the mycobacterial outer membrane: cryo-electron

tomography and vitreous sections reveal the lipid bilayer structure. Proc Natl Acad Sci USA **105**:3963–3967.

14. **Jarlier V**, **Nikaido H**. 1990. Permeability barrier to hydrophilic solutes in Mycobacterium chelonei. J Bacteriol **172**:1418–1423.

15. **Sarathy J**, **Dartois V**, **Dick T**, **Gengenbacher M**. 2013. Reduced Drug Uptake in Phenotypically Resistant Nutrient-Starved Nonreplicating Mycobacterium tuberculosis. Antimicrobial Agents and Chemotherapy **57**:1648–1653.

16. **Batt SM**, **Burke CE**, **Moorey AR**, **Besra GS**. 2020. Antibiotics and resistance: the two-sided coin of the mycobacterial cell wall. Cell Surf **6**:100044.

17. **Bhamidi S**, **Shi L**, **Chatterjee D**, **Belisle JT**, **Crick DC**, **McNeil MR**. 2012. A bioanalytical method to determine the cell wall composition of Mycobacterium tuberculosis grown in vivo. ANALYTICAL BIOCHEMISTRY **421**:240–249.

18. **Betts JC**, **Lukey PT**, **Robb LC**, **McAdam RA**, **Duncan K**. 2002. Evaluation of a nutrient starvation model of Mycobacterium tuberculosis persistence by gene and protein expression profiling. Mol Microbiol **43**:717–731.

19. **Sarathy JP**, **Via LE**, **Weiner D**, **Blanc L**, **Boshoff H**, **Eugenin EA**, **Clifton BE III**, **Dartois VA**. 2018. Extreme Drug Tolerance of Mycobacterium tuberculosis in Caseum. Antimicrobial Agents and Chemotherapy **62**:2149.

20. **Xie Z**, **Siddiqi N**, **Rubin EJ**. 2005. Differential Antibiotic Susceptibilities of Starved Mycobacterium tuberculosis Isolates. Antimicrobial Agents and Chemotherapy **49**:4778–4780.

21. **Liu Y**, **Tan S**, **Huang L**, **Abramovitch RB**, **Rohde KH**, **Zimmerman MD**, **Chen C**, **Dartois V**, **VanderVen BC**, **Russell DG**. 2016. Immune activation of the host cell induces drug tolerance in Mycobacterium tuberculosis both in vitro and in vivo. J Exp Med **213**:809–825.

22. **Dulberger CL**, **Rubin EJ**, **Boutte CC**. 2020. The mycobacterial cell envelope - a moving target. Nature Reviews Microbiology **18**:47–59.

23. **Boutte CC**, **Baer CE**, **Papavinasasundaram K**, **Liu W**, **Chase MR**, **Meniche X**, **Fortune SM**, **Sassetti CM**, **Ioerger TR**, **Rubin EJ**, **Laub M**. 2016. A cytoplasmic peptidoglycan amidase homologue controls mycobacterial cell wall synthesis. eLife **5**:e14590.

24. **Echenique J**, **Kadioglu A**, **Romao S**, **Andrew PW**, **Trombe MC**. 2004.

Protein Serine/Threonine Kinase StkP Positively Controls Virulence and Competence in Streptococcus pneumoniae. Infection and immunity **72**:2434–2437.

25. **Juris SJ**, **Rudolph AE**, **Huddler D**, **Orth K**, **Dixon JE**. 2000. A distinctive role for the Yersinia protein kinase: actin binding, kinase activation, and cytoskeleton disruption. Proceedings of the National Academy of Sciences **97**:9431–9436.

26. **Galyov EE**, **Håkansson S**, **Forsberg Å**, **Wolf-Watz H**. 1993. A secreted protein kinase of Yersinia pseudotuberculosis is an indispensable virulence determinant. Nature **361**:730–732.

27. **Wang J**, **Li C**, **Yang H**, **Mushegian A**, **Jin S**. 1998. A novel serine/threonine protein kinase homologue of Pseudomonas aeruginosa is specifically inducible within the host infection site and is required for full virulence in neutropenic mice. J Bacteriol **180**:6764–6768.

28. **Gee CL**, **Papavinasasundaram KG**, **Blair SR**, **Baer CE**, **Falick AM**, **King DS**, **Griffin JE**, **Venghatakrishnan H**, **Zukauskas A**, **Wei JR**, **Dhiman RK**, **Crick DC**, **Rubin EJ**, **Sassetti CM**, **Alber T**. 2012. A Phosphorylated Pseudokinase Complex Controls Cell Wall Synthesis in Mycobacteria. Science Signaling **5**:ra7–ra7.

29. **Av-Gay Y**, **Everett M**. 2000. The eukaryotic-like Ser/Thr protein kinases of Mycobacterium tuberculosis. Trends Microbiol **8**:238–244.

30. **Cole ST**, **Brosch R**, **Parkhill J**, **Garnier T**, **Churcher C**, **Harris D**, **Gordon SV**, **Eiglmeier K**, **Gas S**, **Barry CE**, **Tekaia F**, **Badcock K**, **Basham D**, **Brown D**, **Chillingworth T**, **Connor R**, **Davies R**, **Devlin K**, **Feltwell T**, **Gentles S**, **Hamlin N**, **Holroyd S**, **Hornsby T**, **Jagels K**, **Krogh A**, **McLean J**, **Moule S**, **Murphy L**, **Oliver K**, **Osborne J**, **Quail MA**, **Rajandream MA**, **Rogers J**, **Rutter S**, **Seeger K**, **Skelton J**, **Squares R**, **Squares S**, **Sulston JE**, **Taylor K**, **Whitehead S**, **Barrell BG**. 1998. Deciphering the biology of Mycobacterium tuberculosis from the complete genome sequence. Nature **393**:537–544.

31. **Sassetti CM**, **Boyd DH**, **Rubin EJ**. 2003. Genes required for mycobacterial growth defined by high density mutagenesis. Mol Microbiol **48**:77–84.

32. **Kang C-M**, **Abbott DW**, **Park ST**, **Dascher CC**, **Cantley LC**, **Husson RN**. 2005. The Mycobacterium tuberculosis serine/threonine kinases PknA and PknB: substrate identification and regulation of cell shape. Genes & Development **19**:1692–1704.

33. **Fernandez P**, **Saint-Joanis B**, **Barilone N**, **Jackson M**, **Gicquel B**, **Cole ST**, **Alzari PM**. 2006. The Ser/Thr Protein Kinase PknB Is Essential for

Sustaining Mycobacterial Growth. J Bacteriol **188**:7778–7784.

34. **Kusebauch U**, **Ortega C**, **Ollodart A**, **Rogers RS**, **Sherman DR**, **Moritz RL**, **Grundner C**. 2014. Mycobacterium tuberculosis supports protein tyrosine phosphorylation. Proceedings of the National Academy of Sciences **111**:9265–9270.

35. **Molle V**, **Brown AK**, **Besra GS**, **Cozzone AJ**, **Kremer L**. 2006. The Condensing Activities of the Mycobacterium tuberculosisType II Fatty Acid Synthase Are Differentially Regulated by Phosphorylation. J Biol Chem **281**:30094–30103.

36. **Slama N**, **Leiba J**, **Eynard N**, **Daffé M**, **Kremer L**, **Quémard A**, **Molle V**. 2011. Negative regulation by Ser/Thr phosphorylation of HadAB and HadBC dehydratases from Mycobacterium tuberculosis type II fatty acid synthase system. Biochemical and Biophysical Research Communications **412**:401–406.

37. **Khan S**, **Nagarajan SN**, **Parikh A**, **Samantaray S**, **Singh A**, **Kumar D**, **Roy RP**, **Bhatt A**, **Nandicoori VK**. 2010. Phosphorylation of enoyl-acyl carrier protein reductase InhA impacts mycobacterial growth and survival. J Biol Chem **285**:37860–37871.

38. **Vilchèze C**, **Molle V**, **Carrère-Kremer S**, **Leiba J**, **Mourey L**, **Shenai S**, **Baronian G**, **Tufariello J**, **Hartman T**, **Veyron-Churlet R**, **Trivelli X**, **Tiwari S**, **Weinrick B**, **Alland D**, **Guérardel Y**, **Jacobs WR**, **Kremer L**. 2014. Phosphorylation of KasB regulates virulence and acid-fastness in Mycobacterium tuberculosis. PLoS Pathog **10**:e1004115.

39. **Veyron-Churlet R**, **Zanella-Cléon I**, **Cohen-Gonsaud M**, **Molle V**, **Kremer L**. 2010. Phosphorylation of the Mycobacterium tuberculosis beta-ketoacyl-acyl carrier protein reductase MabA regulates mycolic acid biosynthesis. J Biol Chem **285**:12714–12725.

40. **Marquardt JL**, **Siegele DA**, **Kolter R**, **Walsh CT**. 1992. Cloning and sequencing of Escherichia coli murZ and purification of its product, a UDP-N-acetylglucosamine enolpyruvyl transferase. J Bacteriol **174**:5748–5752.

41. **Turapov O**, **Forti F**, **Kadhim B**, **Ghisotti D**, **Sassine J**, **Straatman-Iwanowska A**, **Bottrill AR**, **Moynihan PJ**, **Wallis R**, **Barthe P**, **Cohen-Gonsaud M**, **Ajuh P**, **Vollmer W**, **Mukamolova GV**. 2018. Two Faces of CwlM, an Essential PknB Substrate, in Mycobacterium tuberculosis. CellReports **25**:57–67.e5.

42. **Iswahyudi**, **Mukamolova GV**, **Straatman-Iwanowska AA**, **Allcock N**, **Ajuh P**, **Turapov O**, **O'Hare HM**. 2019. Mycobacterial phosphatase PstP regulates global serine threonine phosphorylation and cell division.

Scientific Reports **9**:8337.

43. **Sharma AK**, **Arora D**, **Singh LK**, **Gangwal A**, **Sajid A**, **Molle V**, **Singh Y**, **Nandicoori VK**. 2016. Serine/Threonine Protein Phosphatase PstP of Mycobacterium tuberculosis Is Necessary for Accurate Cell Division and Survival of Pathogen. J Biol Chem **291**:24215–24230.

44. **DeJesus MA**, **Gerrick ER**, **Xu W**, **Park SW**, **Long JE**, **Boutte CC**, **Rubin EJ**, **Schnappinger D**, **Ehrt S**, **Fortune SM**, **Sassetti CM**, **Ioerger TR**. 2017. Comprehensive Essentiality Analysis of the Mycobacterium tuberculosis Genome via Saturating Transposon Mutagenesis. mBio **8**.

45. **Chopra P**, **Singh B**, **Singh R**, **Vohra R**, **Koul A**, **Meena LS**, **Koduri H**, **Ghildiyal M**, **Deol P**, **Das TK**, **Tyagi AK**, **Singh Y**. 2003. Phosphoprotein phosphatase of Mycobacterium tuberculosis dephosphorylates serine–threonine kinases PknA and PknB. Biochemical and Biophysical Research Communications **311**:112–120.

46. **Barford D**. 1996. Molecular mechanisms of the protein serine/threonine phosphatases. Trends Biochem Sci **21**:407–412.

47. **Cohen P**. 1989. The structure and regulation of protein phosphatases. Annu Rev Biochem **58**:453–508.

48. **Mougous JD**, **Gifford CA**, **Ramsdell TL**, **Mekalanos JJ**. 2007. Threonine phosphorylation post-translationally regulates protein secretion in Pseudomonas aeruginosa. Nat Cell Biol **9**:797–803.

49. **Irmler A**, **Forchhammer K**. 2001. A PP2C-type phosphatase dephosphorylates the PII signaling protein in the cyanobacterium Synechocystis PCC 6803. Proceedings of the National Academy of Sciences **98**:12978–12983.

50. **Bradshaw N**, **Losick R**. 2015. Asymmetric division triggers cell-specific gene expression through coupled capture and stabilization of a phosphatase. eLife **4**.

51. **Bradshaw N**, **Levdikov VM**, **Zimanyi CM**, **Gaudet R**, **Wilkinson AJ**, **Losick R**. 2017. A widespread family of serine/threonine protein phosphatases shares a common regulatory switch with proteasomal proteases. eLife **6:e26111**.

52. **Lu G**, **Wang Y**. 2008. Functional diversity of mammalian type 2C protein phosphatase isoforms: new tales from an old family. Clin Exp Pharmacol Physiol **35**:107–112.

53. **Vijay K**, **Brody MS**, **Fredlund E**, **Price CW**. 2000. A PP2C phosphatase containing a PAS domain is required to convey signals of energy stress to

the sigmaB transcription factor of Bacillus subtilis. Mol Microbiol **35**:180–188.

54. **Pullen KE**, **Ng H-L**, **Sung P-Y**, **Good MC**, **Smith SM**, **Alber T**. 2004. An Alternate Conformation and a Third Metal in PstP/Ppp, the M. tuberculosis PP2C-Family Ser/Thr Protein Phosphatase. Structure **12**:1947–1954.

55. **Sajid A**, **Arora G**, **Gupta M**, **Upadhyay S**, **Nandicoori VK**, **Singh Y**. 2011. Phosphorylation of Mycobacterium tuberculosis Ser/Thr Phosphatase by PknA and PknB. PLoS ONE **6**:e17871–11.

56. **Sharma K**, **Gupta M**, **Krupa A**, **Srinivasan N**, **Singh Y**. 2006. EmbR, a regulatory protein with ATPase activity, is a substrate of multiple serine/threonine kinases and phosphatase in Mycobacterium tuberculosis. FEBS J **273**:2711–2721.

57. **Durán R**, **Villarino A**, **Bellinzoni M**, **Wehenkel A**, **Fernandez P**, **Boitel B**, **Cole ST**, **Alzari PM**, **Cerveñansky C**. 2005. Conserved autophosphorylation pattern in activation loops and juxtamembrane regions of Mycobacterium tuberculosis Ser/Thr protein kinases. Biochemical and Biophysical Research Communications **333**:858–867.

58. **Boitel B**, **Ortiz-Lombardía M**, **Durán R**, **Pompeo F**, **Cole ST**, **Cerveñansky C**, **Alzari PM**. 2003. PknB kinase activity is regulated by phosphorylation in two Thr residues and dephosphorylation by PstP, the cognate phospho-Ser/Thr phosphatase, in Mycobacterium tuberculosis. Mol Microbiol **49**:1493–1508.

59. **Veyron-Churlet R**, **Zanella-Cléon I**. 2010. Phosphorylation of the Mycobacterium tuberculosis β-ketoacyl-acyl carrier protein reductase MabA regulates mycolic acid biosynthesis. J. Biol. Chem. **284.** 12714-12725.

60. **Molle V**, **Gulten G**, **Vilchèze C**, **Veyron-Churlet R**, **Zanella-Cléon I**, **Sacchettini JC**, **Jacobs WR Jr.**, **Kremer L**. 2010. Phosphorylation of InhA inhibits mycolic acid biosynthesis and growth of Mycobacterium tuberculosis. Mol Microbiol **78**:1591–1605.

61. **Vilchèze C**, **Hards K**, **Berney M**, **Cook GM**, **Hartman T**. 2014. Energetics of Respiration and Oxidative Phosphorylation in Mycobacteria. Microbiology Spectrum **2**.

62. **Hartmans S**, **De Bont J**. 1992. The genus Mycobacterium—Nonmedical In The Prokaryotes. 2nd ed. Springer-Verlag, New York, NY.

63. **Murphy KC**, **Papavinasasundaram K**, **Sassetti CM**. 2015. Mycobacterial recombineering. Methods Mol Biol **1285**:177–199.

64. **Schnappinger D**, **O'Brien KM**, **Ehrt S**. 2015. Construction of conditional knockdown mutants in mycobacteria. Methods Mol Biol **1285**:151–175.

65. **Pashley CA**, **Parish T**. 2003. Efficient switching of mycobacteriophage L5-based integrating plasmids in Mycobacterium tuberculosis. FEMS Microbiology Letters **229**:211–215.

66. **Ducret A**, **Quardokus EM**, **Brun YV**. 2016. MicrobeJ, a tool for high throughput bacterial cell detection and quantitative analysis. Nature Microbiology **1**:671–677.

67. **Kieser KJ**, **Boutte CC**, **Kester JC**, **Baer CE**, **Barczak AK**, **Meniche X**, **Chao MC**, **Rego EH**, **Sassetti CM**, **Fortune SM**, **Rubin EJ**. 2015. Phosphorylation of the Peptidoglycan Synthase PonA1 Governs the Rate of Polar Elongation in Mycobacteria. PLoS Pathog **11**:e1005010.

68. **Gupta M**, **Sajid A**, **Arora G**, **Tandon V**, **Singh Y**. 2009. Forkhead-associated domain-containing protein Rv0019c and polyketide-associated protein PapA5, from substrates of serine/threonine protein kinase PknB to interacting proteins of Mycobacterium tuberculosis. J Biol Chem **284**:34723–34734.

69. **Cottin V**, **Van Linden A**, **Riches DW**. 1999. Phosphorylation of tumor necrosis factor receptor CD120a (p55) by p42(mapk/erk2) induces changes in its subcellular localization. J Biol Chem **274**:32975–32987.

70. **Su J**, **Forchhammer K**. 2013. Determinants for substrate specificity of the bacterial PP2C protein phosphatase tPphA from Thermosynechococcus elongatus. FEBS J **280**:694–707.

71. **Greenstein AE**, **Grundner C**, **Echols N**, **Gay LM**, **Lombana TN**, **Miecskowski CA**, **Pullen KE**, **Sung P-Y**, **Alber T**. 2005. Structure/Function Studies of Ser/Thr and Tyr Protein Phosphorylation in Mycobacterium tuberculosis. J Mol Microbiol Biotechnol **9**:167–181.

72. **Schlicker C**, **Fokina O**, **Kloft N**, **Grüne T**, **Becker S**, **Sheldrick GM**, **Forchhammer K**. 2008. Structural Analysis of the PP2C Phosphatase tPphA from Thermosynechococcus elongatus: A Flexible Flap Subdomain Controls Access to the Catalytic Site. Journal of Molecular Biology **376**:570–581.

73. **Wu M-L**, **Chan CL**, **Dick T**. 2016. Rel Is Required for Morphogenesis of Resting Cells in Mycobacterium smegmatis. Front Microbiol **7**:1100–10.

74. **Kuru E**, **Hughes HV**, **Brown PJ**, **Hall E**, **Tekkam S**, **Cava F**, **de Pedro MA**, **Brun YV**, **VanNieuwenhze MS**. 2012. In Situ Probing of Newly Synthesized Peptidoglycan in Live Bacteria with Fluorescent D-Amino Acids. Angew Chem Int Ed **51**:12519–12523.

75. **Kamariza M**, **Shieh P**, **Ealand CS**, **Peters JS**, **Chu B**, **Rodriguez-Rivera FP**, **Babu Sait MR**, **Treuren WV**, **Martinson N**, **Kalscheuer R**, **Kana BD**, **Bertozzi CR**. 2018. Rapid detection of Mycobacterium tuberculosis in sputum with a solvatochromic trehalose probe. Sci Transl Med **10**:eaam6310.

76. **Baranowski C**, **Welsh MA**, **Sham L-T**, **Eskandarian HA**, **Lim HC**, **Kieser KJ**, **Wagner JC**, **McKinney JD**, **Fantner GE**, **Ioerger TR**, **Walker S**, **Bernhardt TG**, **Rubin EJ**, **Rego EH**. 2018. Maturing Mycobacterium smegmatis peptidoglycan requires non-canonical crosslinks to maintain shape. eLife **7**:100.

77. **García-Heredia A**, **Pohane AA**, **Melzer ES**, **Carr CR**, **Fiolek TJ**, **Rundell SR**, **Lim HC**, **Wagner JC**, **Morita YS**, **Swarts BM**, **Siegrist MS**. 2018. Peptidoglycan precursor synthesis along the sidewall of pole-growing mycobacteria. eLife **7**.

78. **Deb C**, **Lee C-M**, **Dubey VS**, **Daniel J**, **Abomoelak B**, **Sirakova TD**, **Pawar S**, **Rogers L**, **Kolattukudy PE**. 2009. A Novel In Vitro Multiple-Stress Dormancy Model for Mycobacterium tuberculosis Generates a Lipid-Loaded, Drug-Tolerant, Dormant Pathogen. PLoS ONE **4**:e6077.

79. **Zhang Y**. 2004. Persistent and dormant tubercle bacilli and latent tuberculosis. Front Biosci **9**:1136–1156.

80. **Wayne LG**, **Hayes LG**. 1996. An In Vitro Model for Sequential Study of Shiftdown of. Infection and immunity **64**:2062–2069.

81. **Cordillot M**, **Dubee V**, **Triboulet S**, **Dubost L**, **Marie A**, **Hugonnet JE**, **Arthur M**, **Mainardi JL**. 2013. In Vitro Cross-Linking of Mycobacterium tuberculosis Peptidoglycan by L,D-Transpeptidases and Inactivation of These Enzymes by Carbapenems. Antimicrobial Agents and Chemotherapy **57**:5940–5945.

82. **Liechti GW**, **Kuru E**, **Hall E**, **Kalinda A**, **Brun YV**, **VanNieuwenhze M**, **Maurelli AT**. 2014. A new metabolic cell-wall labelling method reveals peptidoglycan in Chlamydia trachomatis. Nature **506**:507–510.

83. **Feng Z**, **Barletta RG**. 2003. Roles of Mycobacterium smegmatis D-alanine:D-alanine ligase and D-alanine racemase in the mechanisms of action of and resistance to the peptidoglycan inhibitor D-cycloserine. Antimicrobial Agents and Chemotherapy **47**:283–291.

84. **Marrakchi H**, **Lanéelle G**, **Quémard AK**. 2000. InhA, a target of the antituberculous drug isoniazid, is involved in a mycobacterial fatty acid elongation system, FAS-II. Microbiology (Reading, Engl) **146 (Pt 2)**:289–296.

85. **Brogden RN**, **Carmine AA**, **Heel RC**, **Speight TM**, **Avery GS**. 1982. Trimethoprim: a review of its antibacterial activity, pharmacokinetics and therapeutic use in urinary tract infections. Drugs **23**:405–430.

86. **Hancock RE**, **Bell A**. 1988. Antibiotic uptake into gram-negative bacteria. Eur J Clin Microbiol Infect Dis **7**:713–720.

87. **Neuhaus FC**, **Hammes WP**. 1981. Inhibition of cell wall biosynthesis by analogues and alanine. Pharmacol Ther **14**:265–319.

88. **Stephan J**, **Mailaender C**, **Etienne G**, **Daffé M**, **Niederweis M**. 2004. Multidrug resistance of a porin deletion mutant of Mycobacterium smegmatis. Antimicrobial Agents and Chemotherapy **48**:4163–4170.

89. **Ortega C**, **Liao R**, **Anderson LN**, **Rustad T**, **Ollodart AR**, **Wright AT**, **Sherman DR**, **Grundner C**. 2014. Mycobacterium tuberculosis Ser/Thr Protein Kinase B Mediates an Oxygen-Dependent Replication Switch. Plos Biol **12**:e1001746–11.

90. **Arora D**, **Chawla Y**, **Malakar B**, **Singh A**, **Nandicoori VK**. 2018. The transpeptidase PbpA and noncanonical transglycosylase RodA of Mycobacterium tuberculosis play important roles in regulating bacterial cell lengths. J Biol Chem **293**:6497–6516.

91. **Kaur P**, **Rausch M**, **Malakar B**, **Watson U**, **Damle NP**, **Chawla Y**, **Srinivasan S**, **Sharma K**, **Schneider T**, **Jhingan GD**, **Saini D**, **Mohanty D**, **Grein F**, **Nandicoori VK**. 2019. LipidII interaction with specific residues of Mycobacterium tuberculosis PknB extracytoplasmic domain governs its optimal activation. Nature Communications **10**:7470–17.

92. **Le N-H**, **Locard-Paulet M**, **Stella A**, **Tomas N**, **Molle V**, **Burlet-Schiltz O**, **Daffé M**, **Marrakchi H**. 2020. The protein kinase PknB negatively regulates biosynthesis and trafficking of mycolic acids in mycobacteria. J Lipid Res **61**:1180–1191.

93. **Veyron-Churlet R**, **Molle V**, **Taylor RC**, **Brown AK**, **Besra GS**, **Zanella-Cléon I**, **Fütterer K**, **Kremer L**. 2009. The Mycobacterium tuberculosis beta-ketoacyl-acyl carrier protein synthase III activity is inhibited by phosphorylation on a single threonine residue. J Biol Chem **284**:6414–6424.

94. **Li K-K**, **Qu D-H**, **Zhang H-N**, **Chen F-Y**, **Xu L**, **Wang M-Y**, **Su H-Y**, **Tao S-C**, **Wu F-L**. 2020. Global discovery the PstP interactions using Mtb proteome microarray and revealing novel connections with EthR. J Proteomics **215**:103650.

95. **Bollen M**, **Peti W**, **Ragusa MJ**, **Beullens M**. 2010. The extended PP1 toolkit: designed to create specificity. Trends Biochem Sci **35**:450–458.

96. **Roy J**, **Cyert MS**. 2009. Cracking the phosphatase code: docking interactions determine substrate specificity. Science Signaling **2**:re9–re9.

97. **Lin K**, **Hwang PK**, **Fletterick RJ**. 1997. Distinct phosphorylation signals converge at the catalytic center in glycogen phosphorylases. Structure **5**:1511–1523.

98. **García-Heredia A**, **Pohane AA**, **Melzer ES**, **Carr CR**, **Fiolek TJ**, **Rundell SR**, **Lim HC**, **Wagner JC**, **Morita YS**, **Swarts BM**, **Siegrist MS**. 2018. Peptidoglycan precursor synthesis along the sidewall of pole-growing mycobacteria. eLife **7**.

99. **Harth G**, **Lee BY**, **Wang J**, **Clemens DL**, **Horwitz MA**. 1996. Novel insights into the genetics, biochemistry, and immunocytochemistry of the 30-kilodalton major extracellular protein of Mycobacterium tuberculosis. Infection and immunity **64**:3038–3047.

100. **Viljoen A**, **Viela F**, **Kremer L**, **ne YFDX**. 2020. Fast chemical force microscopy demonstrates that glycopeptidolipids define nanodomains of varying hydrophobicity on mycobacteria. Nanoscale Horizons **5**:944–953.

101. **Xu Z**, **Meshcheryakov VA**, **Poce G**, **Chng S-S**. 2017. MmpL3 is the flippase for mycolic acids in mycobacteria. Proceedings of the National Academy of Sciences **114**:7993–7998.

102. **Mailaender C**, **Reiling N**, **Engelhardt H**, **Bossmann S**, **Ehlers S**, **Niederweis M**. 2004. The MspA porin promotes growth and increases antibiotic susceptibility of both Mycobacterium bovis BCG and Mycobacterium tuberculosis. Microbiology (Reading, Engl) **150**:853–864.

103. **Bhaskara GB**, **Wong MM**, **Verslues PE**. 2019. The flip side of phospho□signalling: Regulation of protein dephosphorylation and the protein phosphatase 2Cs. Plant Cell Environ **42**:2913–2930.

Figure S1

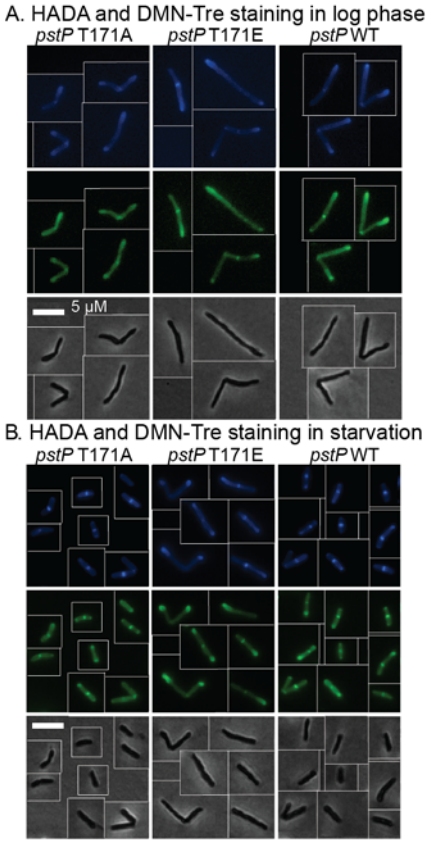

(A) and (B) Representative micrographs of log. phase cells (A) and starved cells in HdB with no glycerol (B) from *pstP* allele strains (WT, T17A and T171E) stained with the fluorescent dyes HADA (blue) and DMN-Tre (green). Corresponding phase images are shown on the bottom panel. The scale bar applies to all images.

Figure S2

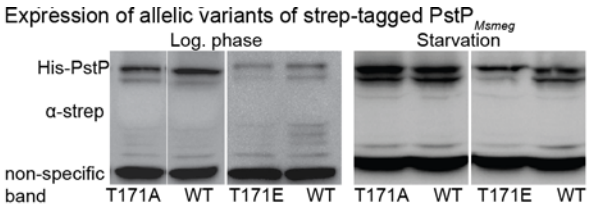

Figure S2: α-strep Western blots of allelic variants of strep-tagged $PstP_{Msmeg}$ in log. (left panel) and starvation phase (right panel). A non-specific band at the bottom in all strains was seen in the blots.